International Journal of Heat and Mass Transfer 220 (2024) 124953

Contents lists available at ScienceDirect

International Journal of Heat and Mass Transfer

journal homepage: www.elsevier.com/locate/ijhmt

Supercritical heat transfer of CO_2 in horizontal tube emphasizing pseudo-boiling and stratification effects

Liangyuan Cheng [a], Qingyang Wang [a,b], Jinliang Xu [a,b,*]

[a] Beijing Key Laboratory of Multiphase Flow and Heat Transfer for Low Grade Energy Utilization, North China Electric Power University, Beijing 102206, China
[b] Key Laboratory of Power Station Energy Transfer Conversion and System of Ministry of Education, North China Electric Power University, Beijing 102206, China

ARTICLE INFO

Keywords:
Supercritical heat transfer
Three-regime-model
Pseudo-boiling
Stratified-wavy flow

ABSTRACT

Here, we investigate supercritical heat transfer of CO_2 in a 10.0 mm diameter horizontal tube, covering pressures, mass fluxes and heat fluxes in the ranges of (7.531~20.513) MPa, (496.7~1346.2) kg/m^{2}s, and (97.4~400.3) kW/m^2, respectively. It is surprising to find the non-monotonic increase of wall temperatures along the flow direction. Besides, either positive or negative wall temperature differences, ΔT, exist between bottom tube and top tube. The three-regime-model is introduced to explore the mechanisms that trigger the above abnormal findings. The stratified-wavy flow involves a liquid-like (LL) core and a vapor-like (VL) layer on the tube wall. The wavy interface is formed by the two separated phases of LL and VL. The oscillation of wall temperatures is explained by the thermal conduction in the solid wall interacted with the stratified-wavy flow in the tube. Once wall temperatures increase, the local heat flux decreases to decrease the evaporation momentum force, reducing the VL layer thickness to ensure the heat transfer recovery. A regime map clarifies the positive and negative temperature difference runs, and the maximum wall temperature differences are well correlated based on the LL phase Reynolds number, $Re_{LL,ave}$. In the two-phase-like (TPL) regime, the measured heat transfer coefficients significantly deviate from the predictions based on the single-phase fluid assumption. The strong deviation of h_{bot}/h_{top} from 1 indicates both important effects of pseudo-boiling and stratification in horizontal tubes, where h_{bot} and h_{top} are the heat transfer coefficients at the bottom generatrix and the top generatrix, respectively. Based on this work, the pseudo-boiling theory is recommended to deal with the supercritical heat transfer.

1. Introduction

With the global warming issue being an imminent threat to human beings, renewable energies are being extensively sought to replace the traditional fossil fuels. Solar energy is a clean energy source with wide availability, and can be exploited for thermal power generation. The supercritical CO_2 (sCO_2) cycle has wide interests due to its higher efficiency, the easier ability to reach supercritical state, and the better safety due to the chemical inertness of CO_2 [1]. Therefore, the sCO_2 cycle with solar energy as the heat source has great potential to produce electricity from clean energy source with high efficiency [2,3]. In parabolic trough based solar thermal power generation system using sCO_2 cycles, the sCO_2 fluid flows in a horizontal tube and absorbs heat, affecting the cycle efficiency and the safety operation of the thermal system [4]. Understanding of the sCO_2 heat transfer in horizontal tubes is of vital importance.

Compared to available investigations of sCO_2 heat transfer in vertical tubes, the investigations of sCO_2 heated in horizontal tubes are limited. Adebiyi and Hall [5] studied the heat transfer of CO_2 in a horizontal tube with a diameter of 22 mm, and found that wall temperatures at the top generatrix are higher than those at the bottom generatrix, which was attributed to the buoyancy effect. Pidaparti et al. [6] performed experiments with sCO_2 in a 10.9 mm diameter tube, and found that the circumferential wall temperature difference is most notable when the pseudo-critical temperature is in between the wall temperature and the bulk fluid temperature. They attributed this observation to the density difference due to the temperature variation between tube wall and bulk

Abbreviations: DC, direct current; HTC, the heat transfer coefficient; Lb, low reynolds number; LL, liquid-like; sCO_2, supercritical carbon dioxide; TPL, two-phase-like.

* Corresponding author at: Beijing Key Laboratory of Multiphase Flow and Heat Transfer for Low Grade Energy Utilization, North China Electric Power University, Beijing 102206, China.
E-mail address: xjl@ncepu.edu.cn (J. Xu).

https://doi.org/10.1016/j.ijheatmasstransfer.2023.124953
Received 24 April 2023; Received in revised form 8 November 2023; Accepted 10 November 2023

Nomenclature

c_p	specific heat capacity (J/kgK)
d_{in}	inner diameter of the tube (m)
d_{out}	outer diameter of the tube (m)
e_A, e_R, e_S	average, mean absolute and standard deviation
F	force (N)
Fr	Froude number ($\frac{G^2}{\rho_{pc}^2 g d_{in}}$)
G	mass flux (kg/m^{2}s)
g	gravitational acceleration (m/s^2)
h	heat transfer coefficient (kW/m^{2}K)
I	current (A)
i	enthalpy (J/kg)
L	test tube length (m)
m	mass flow rate (kg/s)
$m_{LL}g$	liquid-like fluid gravity force per unit length (N/m)
P	pressure (MPa)
ΔP	differential pressure (kPa)
Pr	Prandtl number (ν_b/α_b)
Q	heating power (W)
q_w	heat flux (W/m^2)
Re	Reynolds number ($\frac{Gd_{in}}{\mu_b}$)
SBO	Supercritical boiling number ($\frac{q_w}{Gi_{pc}}$)
T	temperature (°C)
T^-	the onset of pseudo-boiling temperature (K)
T^+	the termination of pseudo-boiling temperature (K)
ΔT	outer wall temperature difference (°C)
t	time (s)
U	voltage (V)
x	pseudo-vapor quality
z	axial location

Greek symbols

δ	vapor-like film thickness
l	thermal conductivity (W/mK)
m	dynamic viscosity (Pa·s)
ν	kinematic viscosity (m^2/s)
r	density (kg/m^3)
θ	circular angle
α	thermal diffusivity

Subscripts

A	mean relative
ave	average
b	bulk fluid
bot	bottom generatrix
DB	Dittus-Boelter
exp	experimental data
in	inlet
iw	inner wall condition
I	inertia
LL	liquid-like
max	maximum value
M	momentum
out	outlet
ow	outer wall condition
pc	pseudo-critical
pre	prediction value
R	mean absolute
S	root-mean-square relative
top	top generatrix
VL	vapor-like

fluid. Walisch et al. [7] found that the buoyancy effect would be diminished by turbulence under high Reynolds number (*Re*) conditions. Liao and Zhao [8] experimentally studied the heat transfer of sCO_2 in small diameter tubes with diameters ranging from 0.5 to 2.16 mm, and found that buoyancy is still important under large *Re* conditions, and the heat transfer coefficient (HTC) decreases when tube diameter decreases, which is different from the results for large diameter tubes. Tanimizu and Sadr [9] and Kim et al. [10] found that there are no connections between the HTC and the buoyancy effect. The existing HTC correlations are only suitable when the fluid temperatures obviously deviate from the pseudo-critical temperature.

The sCO_2 heat transfer was numerically studied in horizontal tubes. Pu et al. [11] studied the turbulent flow of sCO_2 in a horizontal micro-tube with diameter of 2 mm using the *k*-*ε* model, and found that the influence of buoyancy cannot be neglected even in the fully developed turbulent region. Zhao et al. [12] used FLUENT to evaluate different turbulence models by comparing the predicted wall temperatures with the measured values, and found that the low Reynolds (LB) number *k*-*ε* turbulence model gives better results. Heat transfer deterioration, flow stratification, and secondary flows are observed by the simulations using the RNG *k*-*ε* model [13], the AKN *k*-epsilon model [14], and the direct numerical simulation model [15]. However, most of these papers applied constant heat flux boundary condition at the wall by neglecting the wall thickness. Yang [16] considered the solid wall in their model, and found that the predictions by the stand *k*-*ε* model matches the experimental data well.

The existing literature on sCO_2 heat transfer in horizontal tubes can be summarized as follows: 1) For horizontal tubes, heat transfer difference exists between top wall and bottom wall, which is explained by the buoyancy effect and flow acceleration effect. 2) Experimentally, none of the work reported wall temperature oscillation along the tube; numerically, most papers neglected the tube wall and employed a model with fluid domain only.

As mentioned above, the previous works are mostly based on the single-phase framework. In this work, we take a different path, and use the pseudo-boiling concept to deal with the sCO_2 heat transfer. In subcritical pressures, convective boiling in horizontal tubes has been extensively studied, which contains several two-phase flow patterns: bubbly flow, slug flow, stratified flow, stratified-wavy flow and annular flow [17]. Different flow patterns correspond to different heat transfer mechanisms. Boiling is the dominant mechanism for bubble flow, but convection is the dominant mechanism for annular flow. Especially, for stratified flow and stratified-wavy flow, the bottom wall has a larger possibility to be immersed by liquid, thus better heat transfer is kept there. However, the top wall may be partially dry, thus poor heat transfer is achieved there [18]. The Froude number (*Fr*), which can be written for the liquid phase and vapor phase, can characterize the stratification degree of the two-phase fluid in horizontal tubes [19].

In this work, sCO_2 heat transfer was experimentally investigated in a 10.0 mm diameter tube. The experimental parameters cover wide ranges, including pressures of 7.531~20.513 MPa, mass flux of 496.7~1346.2 kg/m^{2}s, and heat flux of 97.4~400.3 kW/m^2. Wall temperatures are oscillating along the flow direction, and they are different between top wall and bottom tube. Previously, the three-regime-model in supercritical pressure was developed for vertical flows. Here, the three-regime-model is extended to consider the complicated supercritical heat transfer in horizontal tube. The wall temperature oscillation is thought to be caused by the stratified-wavy flow in supercritical pressures, containing liquid-like (LL) phase in the tube core and vapor-like (VL) phase on the tube wall. The non-

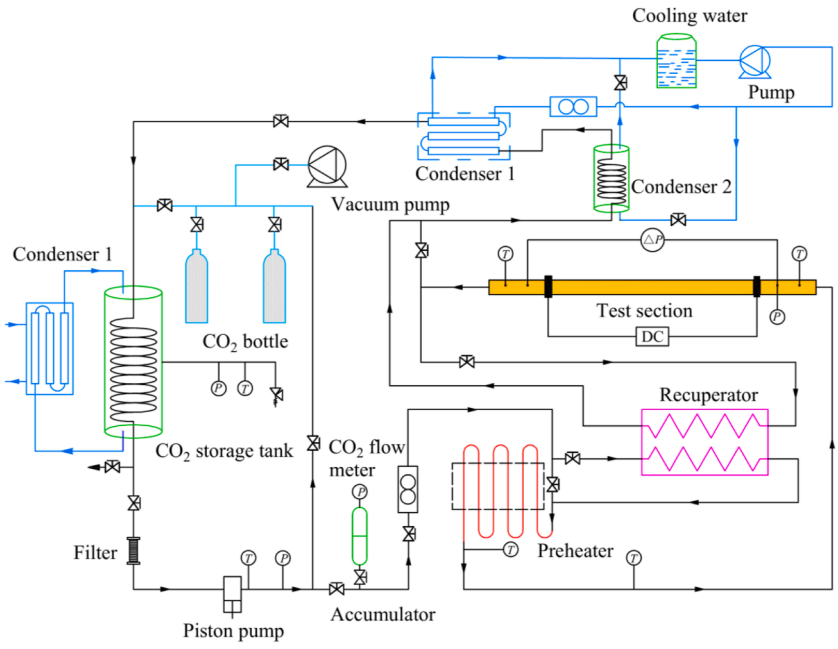

Fig. 1. Experiment setup.

monotonous variation of the vapor-like film thickness is caused by the thermal conduction within the tube wall and the heat transfer in the fluid domain. The general trend shows higher temperatures at the top wall than those at the bottom wall, but inverse trend is also detected due to the coupling of the heat transfer in the solid domain and the fluid domain. Using the pseudo-vapor quality, it is shown that in the two-phase-like (TPL) regime, the heat transfer significantly deviates from the single-phase convection, while in the VL and LL regimes, the heat transfer is close to single-phase convection. Moreover, it is found that the *Fr* number, representing the competition between inertia force and gravity force, can quantify the stratification degree. The large *Fr* case indicates less important of the gravity on the flow, weakening the difference of heat transfer between top wall and bottom wall. This work validates the three-regime-model, and provides important reference for the design and operation of heat exchangers operating in supercritical pressures. This work is especially important for solar receivers because these tubes are usually horizontally positioned.

2. Theoretical background of supercritical heat transfer in horizontal tubes

Before we use the three-regime-model to analyze the supercritical heat transfer in the horizontal tube, a short description of the three-regime-model is given here. the three-regime-model treats the supercritical fluid to contain three regimes of liquid-like (LL), two-phase-like (TPL) and vapor-like (VL) [20]. Either LL or VL is single-phase fluid, but TPL contains a mixture (co-existence) of LL and VL. Hence, the model is based on the multi-phase framework. Ref. [20] presents an integrated strategy to deal with the transition boundaries among the three regimes, the physical properties of each phase in the TPL regime, and a set of non-dimensional parameters. The numerical and experimental techniques existed for subcritical pressure are suggested to treat the supercritical fluid.

The change from LL to TPL is assumed to take place at a temperature of T^-, and the change from TPL to VL is assumed to occur at a temperature of T^+, in which T^- and T^+ are determined by the thermodynamics method [21]. The two transition temperatures can also be predicted by the molecular dynamics approach [22], and they match the thermodynamics approach well. For two-phase flow in subcritical pressure, physical properties are defined for liquid and vapor at the saturation temperature [23,24]. In supercritical pressure, because pseudo-boiling takes place in a temperature range instead of a constant temperature [21], the physical properties for LL and VL are defined at T^- and T^+ respectively.

The pseudo-vapor quality x quantifies the mass content of the VL phase with respect to the total mixture [20]

$$x = \frac{i_b - i_{LL}}{i_{VL} - i_{LL}} \tag{1}$$

where i is the enthalpy. The subscripts b, LL, and VL represent bulk fluid, LL, and VL, respectively. The x is related to the phase regime: $x<0$ represents LL, $0<x<1$ represents TPL, and $x>0$ represents VL.

Once the three-regime-model is applied for horizontal flows, non-dimensional parameters should be defined for bulk fluid, LL phase and VL phase, respectively. The Reynolds number is defined as [20]

$$Re = \frac{Gd_{in}}{\mu_b}, Re_{LL} = \frac{G(1-x)d_{in}}{\mu_{LL}}, Re_{VL} = \frac{Gxd_{in}}{\mu_{VL}} \tag{2}$$

$$Re_{ave} = \frac{Gd_{in}}{\mu_{b,ave}}, Re_{LL,ave} = \frac{G(1-x_{ave})d_{in}}{\mu_{LL}}, Re_{VL,ave} = \frac{Gx_{ave}d_{in}}{\mu_{VL}} \tag{3}$$

where G is the mass flux, d_{in} is the inner diameter of the tube, and μ is the viscosity. We note that Eq. (2) is defined along the flow direction, and Eq. (3) summarizes the average effect over the whole heating section, represented by the subscript ave, μ_{ave} is the viscosity at the average inlet and outlet bulk temperatures ($T_{b,ave}$), $T_{b,ave} = 0.5(T_{in} + T_{out})$; $x_{ave} = 0.5(x_{in} + x_{out})$.

The Froude number is [20]:

$$Fr = \frac{G^2}{\rho_b^2 g d_{in}}, Fr_{LL} = \frac{G^2(1-x)^2}{\rho_{LL}^2 g d_{in}}, Fr_{VL} = \frac{G^2 x^2}{\rho_{VL}^2 g d_{in}} \tag{4}$$

$$Fr_{ave} = \frac{G^2}{\rho_{ave}^2 g d_{in}}, Fr_{LL,ave} = \frac{G^2(1-x_{ave})^2}{\rho_{LL}^2 g d_{in}}, Fr_{VL,ave} = \frac{G^2 x_{ave}^2}{\rho_{VL}^2 g d_{in}} \tag{5}$$

where ρ_{ave} is the density at $T_{b,ave}$.

Since the x monotonically increases along the tube, Eq. (4) calculates the bulk *Fr*, Fr_{LL} and Fr_{VL} for a particular location along the tube, while Eq. (5) calculates the three averaged *Fr* numbers.

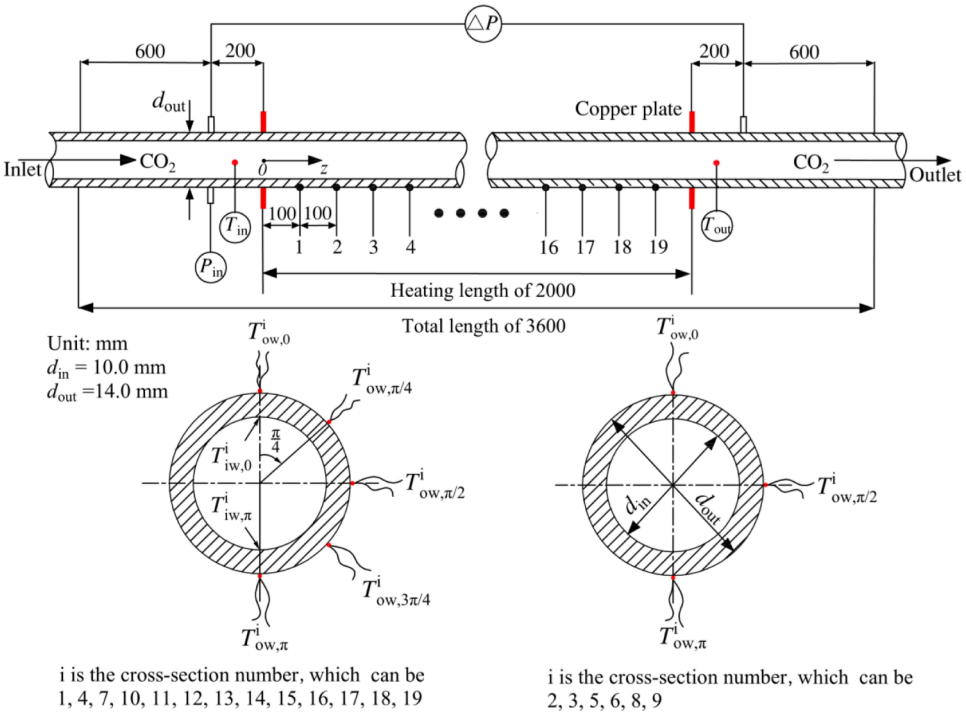

Fig. 2. The horizontal tube used in this study.

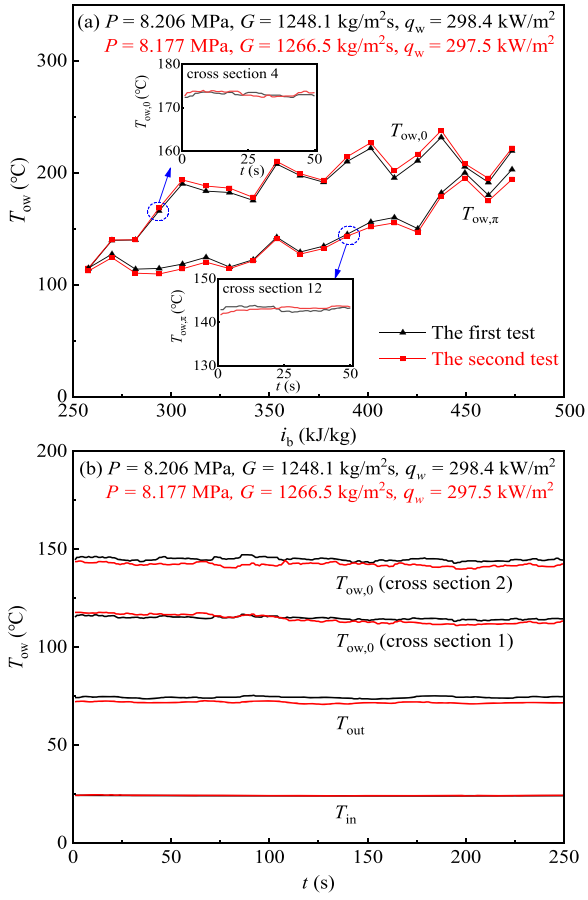

Fig. 3. Verifications of reliability and repeatability of the heat transfer system.

Table 1
Uncertainties and ranges of various parameters.

Value	Measuring instrument	Range	Uncertainty
Mass flux G	DMF−1−3	496.7~1346.2 kg/m^3	2.15 %
Pressure P	Rosemount 1151	7.531~20.513 MPa	0.958 %
Differential pressure ΔP	Rosemount 3051	2.1~23.4 kPa	2.08 %
fluid temperature T_b	K-thermocouple	33.45~190.42 °C	0.5 °C
Outer wall temperature T_{ow}	K-thermocouple	21.71~370.49 °C	0.5 °C
Total quantity of heat Q		1.88~23.25kW	3.43 %
Heat flux q_w		97.42~402.25 kW/m^2	5.05 %
Heat transfer coefficient h		0.732~6.28kW/m^{2}K	5.66 %
Test section voltage U	Precision voltmeter	11.5~23.6V	0.2 %
Test section current I	Precision ammeter	551~1063A	0.2 %

The supercritical boiling number, *SBO*, initially proposed for vertical flows [25], may also be interest for horizontal flows. The *SBO* represents the competition between evaporation momentum force and inertia force [26]:

$$SBO = \frac{q_w}{G i_{pc}} \tag{6}$$

where q_w is the heat flux at the inner wall surface, and i_{pc} is the enthalpy at the pseudo-critical point.

The pseudo-boiling concept has been employed on the heat transfer in vertical tubes [25–27]. In this work, we experimentally studied sCO_2 heat transfer in a horizontal tube. It is interesting to observe oscillations of wall temperatures along the axial coordinate. This finding inspires us to deduce a stratified-wavy pattern in supercritical pressure. The two-phases of VL and LL forms the wavy interface. Because the VL layer thickness dominates the heat transfer between the fluid and the tube

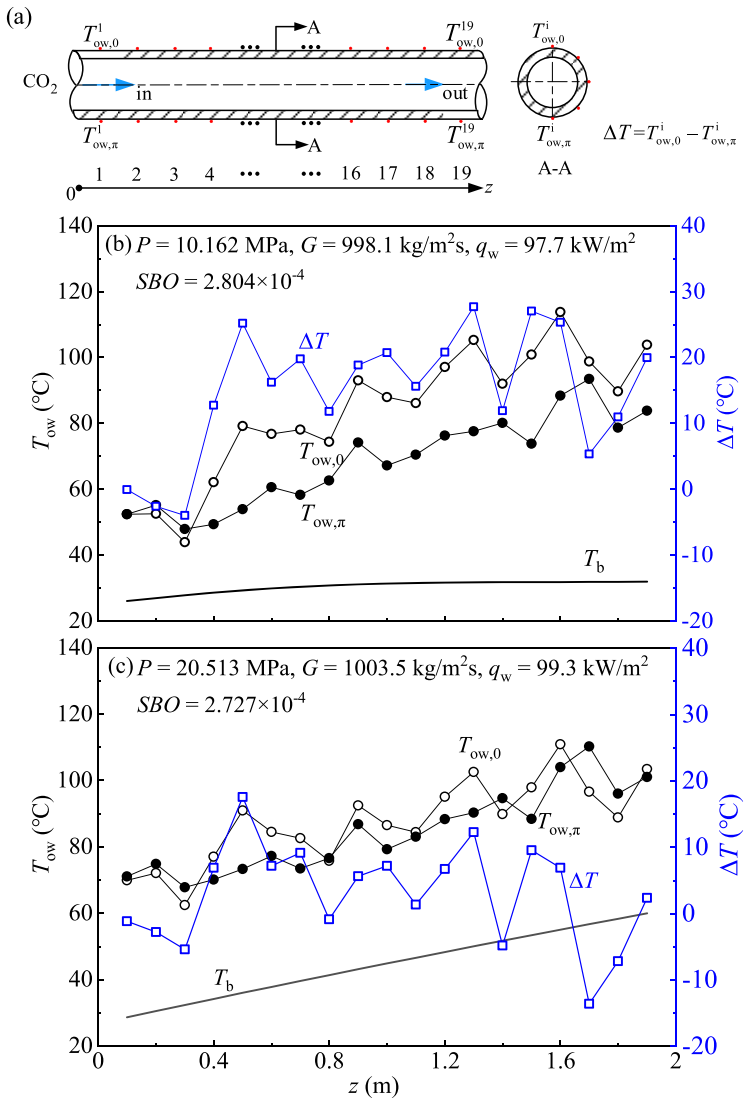

Fig. 4. Outer wall temperature and temperature difference between top generatrix and bottom generatrix along the tube (small *SBO* cases).

wall, an increase of VL thickness elevate the wall temperature along the flow direction. Inversely, the decrease of VL thickness decreases the wall temperatures. Thus, the wavy interface between VL and LL is reasonably proposed due to the axial oscillation of wall temperatures. One shall note that the stratified-wavy flow in subcritical pressure contains liquid on the bottom tube and vapor on the top tube [18], which is different from that in supercritical pressure. The common feature in the two pressure ranges is the wavy interface.

3. Experiments

3.1. Experimental system and test tube

Fig. 1 shows the experimental setup, including a main CO_2 circulation loop, a coolant circulation loop, an electric heating system, and a data acquisition system, which is modified from Ref. [27]. The main loop is vacuumed by a pump to remove the non-condensable gas, and then pressurized with CO_2. The CO_2 fluid leaves the storage tank, passes through a filter, enters the main loop pumped by a piston pump, then passes the preheater and the test section, cools down in the condenser, and finally returns to the storage tank.

The test tube is made of 1Cr18Ni9Ti stainless steel, having a total length of 3600 mm, an inner diameter of 10 mm, and an outer diameter of 14 mm (see Fig. 2). The effective heating length is 2000 mm. There are two adiabatic sections for flow stabilization and measurement before and after the heating section, each having a length of 800 mm. The tube is horizontally arranged during experiments. Direct current is passed through the copper electrode to generate joule heating. Thermocouples are welded on the outer surface of the tube at 19 axial locations spaced 100 mm apart, and each location has either 3 or 5 thermocouples to measure the circumferential temperatures, which are arranged in a semi-circle for each tube cross section due to symmetry (see Fig. 2). Two thermocouples are inserted into the center of the tube to measure the inlet and outlet bulk fluid temperatures, recorded as T_{in} and T_{out} respectively.

To decrease the heat loss to the environment, 50 mm-thick thermal insulation materials are wrapped on the test tube.

3.2. Data reduction

Mass flow rate m, inlet and outlet bulk fluid temperatures T_{in} and T_{out}, and outer wall temperatures of the tube T_{ow}, are obtained by experiments. The mass flux is calculated as

$$G = \frac{4m}{\pi d_{in}^2} \tag{7}$$

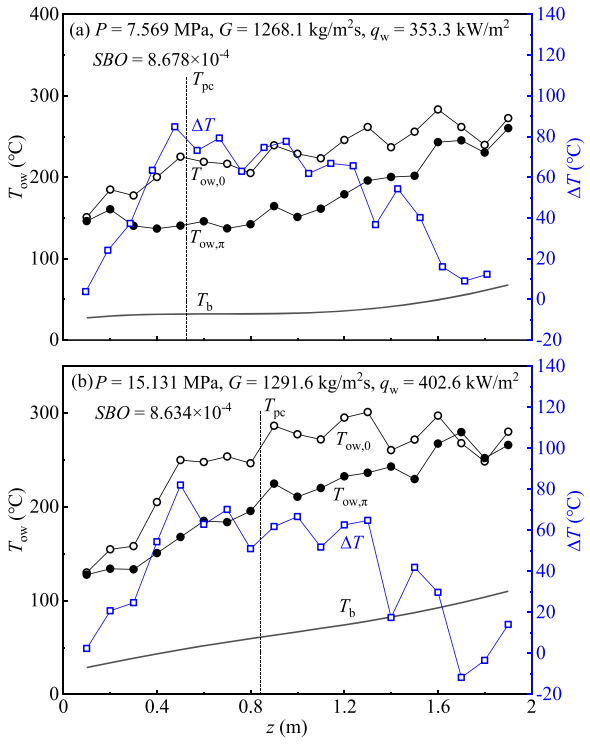

Fig. 5. Outer wall temperature and temperature difference between top generatrix and bottom generatrix along the tube (moderate *SBO* cases).

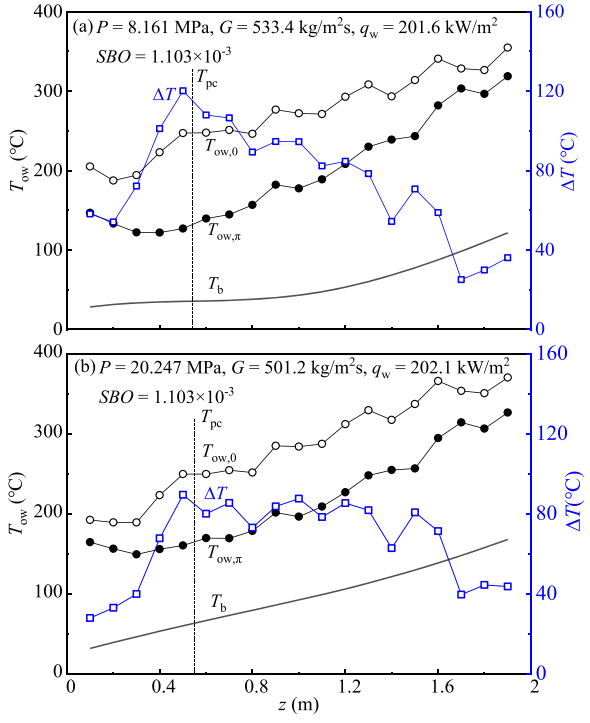

Fig. 6. Outer wall temperature and temperature difference between top generatrix and bottom generatrix along the tube (large *SBO* cases).

The heating power Q is obtained as

$$Q = m(i_{\mathrm{out}} - i_{\mathrm{in}}) \tag{8}$$

where i_{out} and i_{in} are the bulk fluid enthalpies defined by the outlet and inlet fluid temperatures, respectively. In this work, the heating power for each working condition obtained using Eq. (8) is always above 96 % of the supplied electric power, ensuring good thermal insulation. The average wall heat flux q_{w} is obtained as

$$q_{\mathrm{w}} = \frac{Q}{\pi d_{\mathrm{in}} L} \tag{9}$$

where L is the heating length of the tube, noting that q_{w} is the heat flux averaged on the inner wall surface of the heating section. Therefore, for a given axial location z, the bulk fluid enthalpy is

$$i_{\mathrm{b}}(z) = i_{\mathrm{in}} + \frac{q_{\mathrm{w}} \pi d_{\mathrm{in}} z}{m} \tag{10}$$

Once $i_{\mathrm{b}}(z)$ is achieved, the local bulk fluid temperature T_{b} can be decided using the NIST software. An important procedure is to determine the heat transfer coefficients on the inner wall surface, h. Because the horizontal tube involves the non-symmetry distribution of the supercritical fluid, the h is not only varied along the flow direction, but also dependent on the circular angle over the tube cross-section. The inner heat transfer coefficients are determined with the aid of inverse heat conduction theory [28]. The inverse thermal conduction model computes the temperature field under the conditions of the measured discrete temperatures and the thermal insulation boundary on the outer wall surface (see Fig. 2). The prediction accuracy is verified by experiments in Ref. [29]. Once the inner wall temperatures $T^{\mathrm{i}}_{\mathrm{iw},\theta}$ and heat flux $q^{\mathrm{i}}_{\mathrm{iw},\theta}$ are obtained, the local heat transfer coefficient is expressed as

$$h^{\mathrm{i}}_{\mathrm{iw},\theta} = \frac{q^{\mathrm{i}}_{\mathrm{iw},\theta}}{T^{\mathrm{i}}_{\mathrm{iw},\theta} - T_{\mathrm{b}}(z)} \tag{11}$$

where the subscripts of iw and q refer to the inner wall condition and the circular angle, which is 0° at the top generatrix and p at the bottom generatrix, the superscript i means the i$^{\mathrm{th}}$ section along the flow direction.

3.3. System validation and uncertainty analysis

Repeated experiments were performed (see Fig. 3a). Two separate experiments were conducted on different dates with working parameters almost the same, and the resulting wall temperature profiles are almost identical. It is shown that the top point has higher temperature than the bottom point. Later we will show that this is not always true. Under specific conditions, the present work identifies higher temperatures at the bottom tube than those at the top tube. It is observed that the general trend is the increase of the wall temperatures along the flow direction. However, the spatial-oscillation distribution of the wall temperatures is observed, which is also explained latter in this work. Fig. 3(b) shows the temporal evolution of wall temperatures at two different cross sections and the inlet and outlet fluid temperatures, showing stable temperatures over several minutes with minimal fluctuation.

Table 1 summarizes measurement instruments and uncertainties of the measured parameters. The uncertainties of the calculated parameters are also listed in Table 1, which are obtained based on the error propagation principle. For a given parameter Y calculated from directly measured parameters $x_1, x_2, \ldots, x_{\mathrm{N}}$, namely, $Y = f(x_1, x_2, \ldots, x_{\mathrm{N}})$, if uncertainties of the measured parameters are Δx_1, Δx_2, …, Δx_{N}, respectively, the uncertainty for Y can be calculated as

$$\Delta Y = \sqrt{\sum_{\mathrm{i}=1}^{N} \left(\frac{\partial Y}{\partial x_{\mathrm{N}}} \Delta x_{\mathrm{N}} \right)^2} \tag{12}$$

In this work, error analysis is performed to evaluate the effectiveness of new correlations. The mean relative error e_{A}, the mean absolute relative error e_{R}, and the root-mean-square relative error e_{S} are employed, which can be calculated by [30].

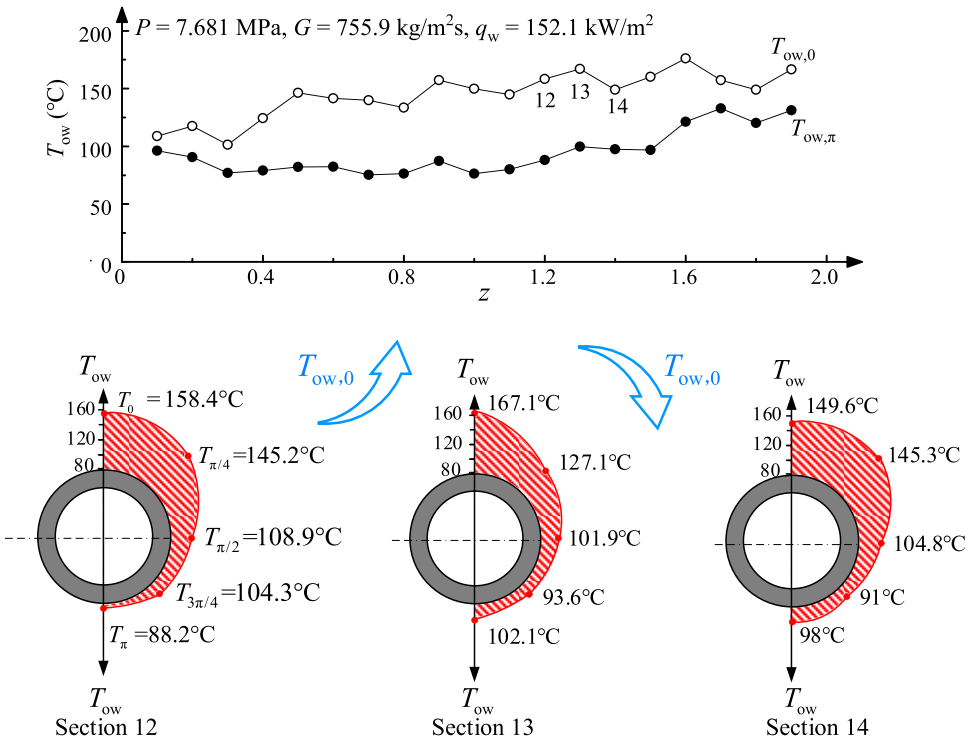

Fig. 7. Axial and circumferential variations of outer wall temperatures.

$$e_A = \frac{1}{n}\sum_{1}^{n} e_i \times 100\% \tag{13}$$

$$e_R = \frac{1}{n}\sum_{1}^{n} |e_i| \times 100\% \tag{14}$$

$$e_S = \sqrt{\frac{1}{n}\sum_{1}^{n} e_i^2 \times 100\%} \tag{15}$$

where the deviation for a single data point e_i is defined as

$$e_i = \left(\frac{x_{i,pre} - x_{i,exp}}{x_{i,exp}}\right) \times 100\% \tag{16}$$

4. Results and discussion

4.1. Wall temperature oscillation

In our earlier work for sCO_2 heat transfer in vertical tubes [26,27,31], it was found that the critical *SBO* exists to quantify the transition from normal heat transfer to heat transfer deterioration. The *SBO* represents the competition between evaporation momentum force and inertia force, in which the former tends to adhere the vapor-like layer on the wall but the latter tends to decrease the vapor-like film thickness. Hence, the *SBO* dominates the vapor-like layer thickness to influence heat transfer. The *SBO* also reflects the comprehensive effect of heat flux and mass flux on heat transfer in horizontal tubes. Figs. 4–6 present the outer wall temperatures at the top generatrix and the bottom generatrix as well as the temperature difference between them along the flow direction, at three groups of small *SBO*, moderate *SBO* and large *SBO*. In the two subfigures of b and c in Fig. 4, and the two subfigures of a and b in Figs. 5 and 6, the working conditions are different but they share similar *SBO* in each figure. Under all these conditions, the oscillation of wall temperatures is observed along the flow direction.

For boiling in horizontal tubes in subcritical pressures, the top wall has higher temperatures than the bottom wall [32]. This is not always true in the present work. Under small and moderate *SBO*s shown in Figs. 4 and 5, negative temperature difference is observed just before the ending of the heating section, but positive temperature difference is kept along the whole heating section at larger *SBO* shown in Fig. 6. The oscillation of wall temperatures and negative wall temperature difference are caused by the coupling of thermal conduction in the solid wall and the phase distribution in the fluid side, which are analyzed latter. Fig. 7 plots the oscillation of outer wall temperatures along the flow direction at $P = 7.681$ MPa, $G = 755.9$ kg/m^{2}s and q_w=152.1 kW/m^2. The outer wall temperatures along the tube circumference are also plotted at the three cross-sections of 12, 13 and 14. It is seen that at the top generatrix, the temperatures increase from 158.4 °C at the section 12 to 167.1 °C at the section 13, but decrease to 149.6 °C at the section 14.

Two-phase flow oscillation under heating condition widely occurs in subcritical pressures, referring to various instabilities versus time, including pressure drop type oscillation [33], density wave oscillation [34], and acoustic oscillation [35]. Here, we report temperature oscillations along the flow direction, but they are stable versus time. The oscillation is caused by the coupling of the thermal conduction in the solid wall and the phase distribution in the tube (see Fig. 8). Based on the observations of wall temperatures along axial and circumferential directions, the flow includes a waved liquid-like snake surrounded by a vapor-like film on the tube wall. At the top generatrix, the outer wall temperature and inner wall heat flux are recorded as $T^{z}_{ow,0}$ and $q^{z}_{iw,0}$, respectively. To understand the axial-variation of various parameters, three axial locations of z, $z+\Delta z$ and $z+2\Delta z$ are paid attention. Considering an increase of the outer wall temperatures from z to $z+\Delta z$, the relationship between the two cross sections is $T^{z+\Delta z}_{ow,0} = T^{z}_{ow,0} + \Delta T_1$, where $\Delta T_1 > 0$. The increase of wall temperature decreases the local heat flux, $q^{z+\Delta z}_{iw,0}$, due to thermal conduction in both axial direction and circumferential direction. At the top generatrix, *SBO* is written as $SBO^{z+\Delta z}_{0} = q^{z+\Delta z}_{iw,0}/(Gi_{pc})$, which decreases due to the thermal conduction effect in the solid wall, decreasing the evaporation momentum force, F_M, hence enhancing the inertia effect, F_I, to shear the wall attached vapor-like film. Thus, the vapor-like film thickness decreases at $z+2\Delta z$, making the heat transfer to recover (see Fig. 8d). Hence, the outer wall

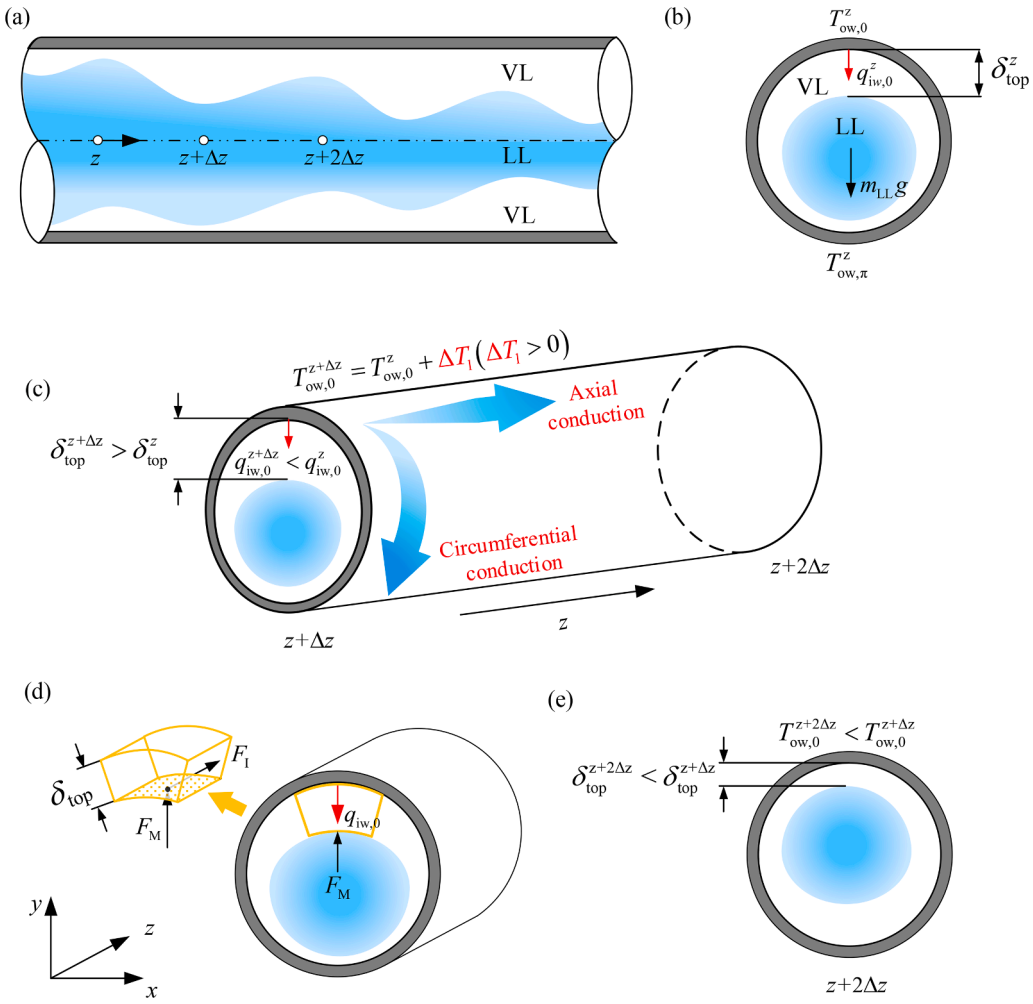

Fig. 8. Newly proposed stratified-wavy flow to adapt the oscillation of wall temperatures along the flow direction. (a) the stratified-wavy flow; (b) definition of parameters over the tube cross section at z. (c) variations of parameters from z+Dz to z + 2Dz. (d) balance between the evaporation momentum force F_M and the inertia force F_I (e) heat transfer recovery at z + 2Dz.

temperature is lowered from z + Δzto z + 2Δz. In summary, the increase of wall temperatures decreases the local heat flux due to the solid thermal conduction. The local *SBO* decreases to decrease the vapor-like layer thickness at the wall, thus the heat transfer can be recovered.

4.2. Non-uniform wall temperature distribution along circumferential direction

Compared with supercritical heat transfer in vertical tubes, strong non-uniform phase distribution exists in horizontal tubes due to the stratification effect, causing non-uniform distribution of wall temperatures along the circumferential direction. The temperature difference between top generatrix and bottom generatrix, recorded as $\Delta T = T^{z}_{ow,0} - T^{z}_{ow,\pi}$, determines the thermal stress to influence the safety of the heat transfer system, especially at high heat fluxes. Here, two questions should be answered. First, over the whole range of the running parameters, some runs have positive ΔT, but some runs have negative ΔT. The question is that where is the transition boundary between the positive ΔT runs and the negative ΔT runs? The second question is that when the running parameters such as operating pressure, mass flux and heat flux are given, how to quantify the temperature difference?

The heat transfer in circumferential direction is influenced by the Froude number. Now that the fluid is treated separately by a liquid-like phase and a vapor-like phase, we use the Froude number defined for the vapor-like, $Fr_{VL,ave}$, and the liquid-like, $Fr_{LL,ave}$, to characterize the transition boundary between the positive ΔT and negative ΔT cases in logarithmic coordinates (see Fig. 9a). A regime map can be clearly established by a transition line, in which data points for the negative ΔT and positive ΔT cases are populated in the left-top region and the right-bottom region, respectively. Larger $Fr_{VL,ave}$ possesses larger inertia effect of the vapor-like phase with respect to gravity, hence the top wall has higher temperatures than the bottom wall. The transition boundary line can be correlated by the following equation.

$$\lg(Fr_{LL,ave}) = 0.58 \times \lg(Fr_{\mathbf{VL,ave}}) + 0.22 \quad (17)$$

In order to understand the wall temperature differences along the flow direction, two runs are selected, one for case a in the negative ΔT region, and the other for case b in the positive ΔT region. Both negative and positive ΔT runs show the non-monotonous variations of the temperature difference. For the negative ΔT run, ΔT is either positive or negative along the flow direction, the negative ΔT can be larger than 10 °C (see Fig. 9b). Alternatively, for the positive ΔT run, ΔT is always larger than 0 (see Fig. 9c). We define ΔT_{max} to quantify the maximum non-uniform degree of wall temperatures. All the data points of ΔT_{max} are summarized in Fig. 10, demonstrating linear and decrease trend versus the Reynolds number defined for the liquid-like phase, $Re_{LL,ave}$, (see Fig. 10a), or linear and increase trend versus the supercritical boiling number, *SBO*, (see Fig. 10b). Two correlations are given as follows:

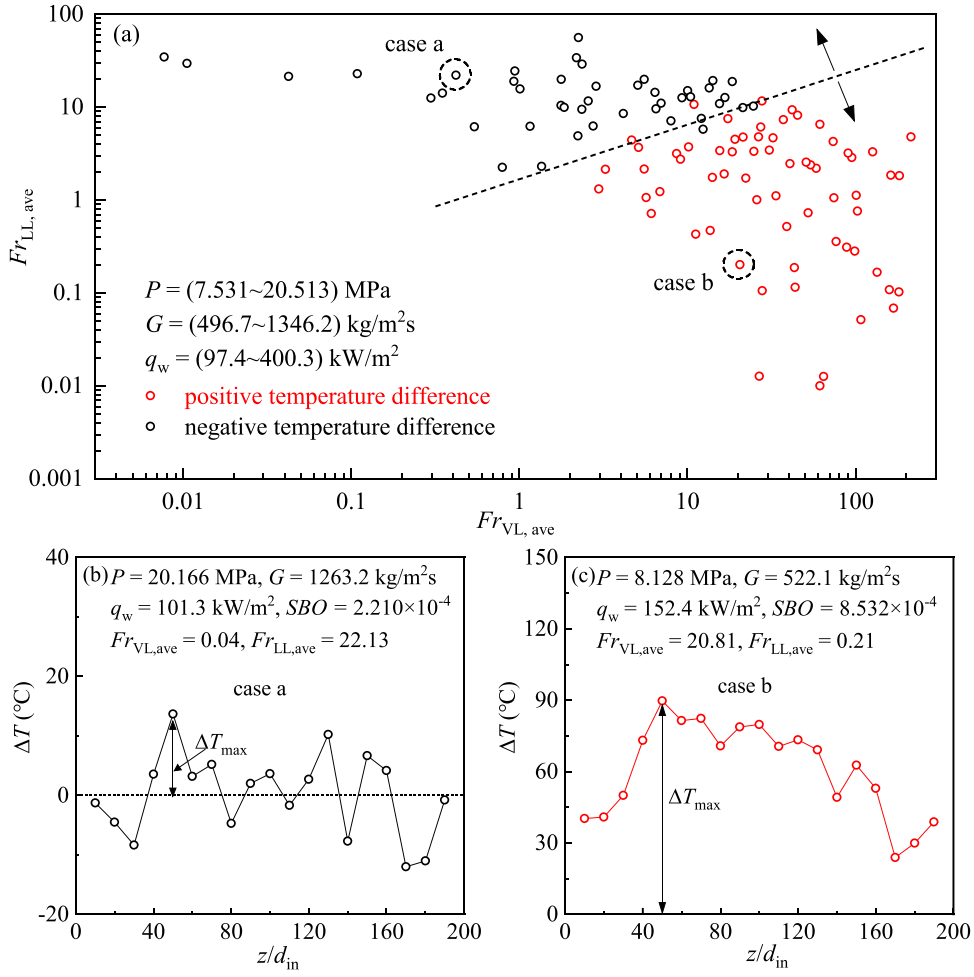

Fig. 9. The regime map to clarify the positive and negative temperature difference runs. (a) the regime map; (b) the negative wall temperature case; (c) the positive wall temperature case.

$$\Delta T_{max} = -4.115 \times 10^{-4} Re_{LL,ave} + 99.3 \quad (18)$$

$$\Delta T_{max} = 1.109 \times 10^{5} SBO - 9.8 \quad (19)$$

Using the error analysis described in the Section 3.3, for Eq. (18), e_A=9.55 %, e_R=28.67 %, and e_S=67.76 %, and for Eq. (19), e_A=5.38 %, e_R=14.35 %, and e_S=26.8 %. This shows that the maximum temperature difference between top and bottom walls are resulted from the thickness of the VL film near the wall. the *SBO* value dominates the VL film thickness near the tube wall by affecting its growth: a larger *SBO* indicates larger evaporation momentum force and thus larger VL film thickness, causing deteriorated heat transfer at the top wall. Meanwhile, because the Re_{LL} represents the competition between inertia force of the LL phase and the viscous force, a larger Re_{LL} indicates larger inertia force of the LL phase, which tends to limit the thickness of the VL layer near the tube wall, and results in smaller circumferential difference of the VL layer thickness. Therefore, both Re_{LL} and *SBO* affect the circumferential heat transfer behavior, resulting in the linear trends of ΔT_{max} against the average Re_{LL} and the *SBO*. Fig. 11 shows that the average Re_{LL} monotonically decreases with increasing *SBO*, suggesting that the two parameters have internal relationship covering the present data range. This is the reason why ΔT_{max} can be correlated by both the $Re_{LL,ave}$ and *SBO* (see Eqs. (18) and (19).

4.3. sCO_2 heat transfer emphasizing the pseudo-boiling effect

Supercritical heat transfer is complex when the fluid temperature is close to the pseudo-critical temperature, either deteriorated or enhanced. According to the three-regime-model, we plot the local heat transfer coefficient against the pseudo-vapor quality *x* defined by Eq. (1) in Fig. 12. The horizontal axis is the *x* value, which increases from subcooled LL ($x<0$) to superheated VL ($x>1$) along the tube. The vertical axis is h_{exp}/h_{DB}, which is the ratio of the experimentally determined heat transfer coefficient, h_{exp}, divided by the Dittus-Boelter correlation determined heat transfer coefficient, h_{DB}. The experimentally obtained *h* for both the top generatrix (h_{top}) and the bottom generatrix (h_{bot}) are obtained based on Eq. (11), and the h_{DB} is obtained as

$$h_{DB} = 0.023 \frac{\lambda_b}{d_{in}} \left(\frac{G d_{in}}{\mu_b} \right)^{0.8} Pr_b^{0.4} \quad (20)$$

where λ_b, μ_b, and Pr_b are evaluated under bulk fluid temperature condition.

In Fig. 12, h_{exp}/h_{DB}=1 means that the experimental heat transfer can be exactly predicted by the DB correlation to obey the single-phase convection, and h_{exp}/h_{DB} deviating from 1 indicates that the experimental heat transfer deviates from the single-phase convection. Fig. 12 shows that with higher pressure of ~20 MPa, the h_{exp}/h_{DB} is closer to 1, indicating that the weakened pseudo-boiling effect at extremely high pressure such as three times of the critical pressure. Moreover, both h_{top}/h_{DB} and h_{bot}/h_{DB} significantly deviate from 1 in the TPL region with *x* in the range of (0–1). The h_{top}/h_{DB} and the h_{bot}/h_{DB} are in the range of 0.043~1.734 and 0.065~1.687, respectively, indicating both significantly deviating from 1. However, in the LL regime with *x* smaller than

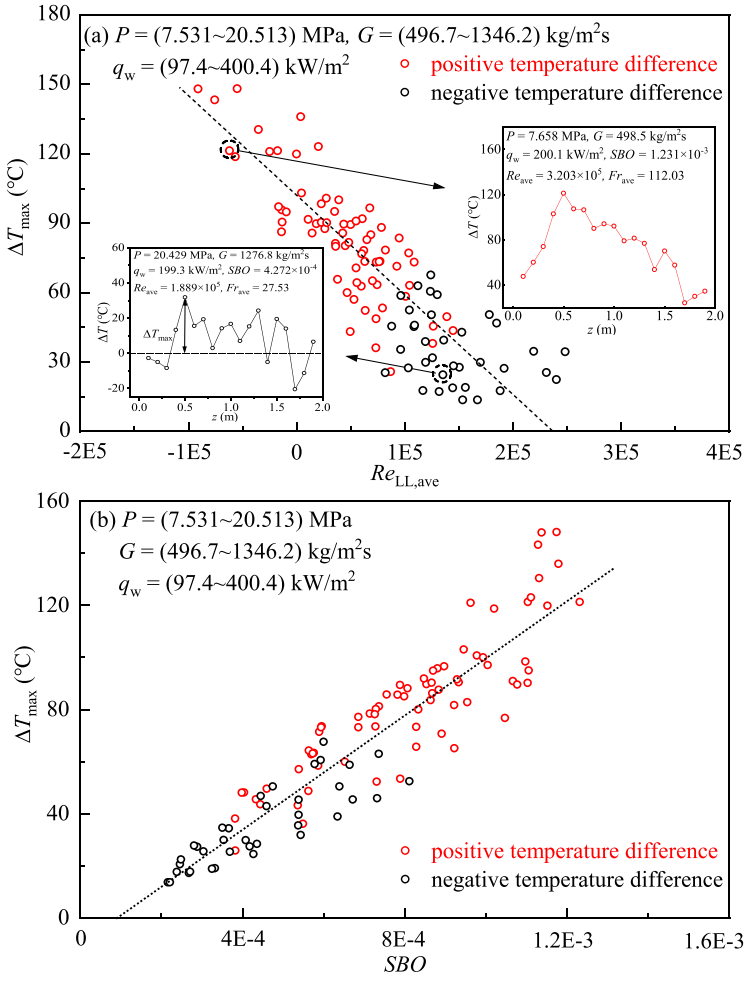

Fig. 10. Maximum wall temperature difference versus $Re_{LL,ave}$ (a) and *SBO* (b).

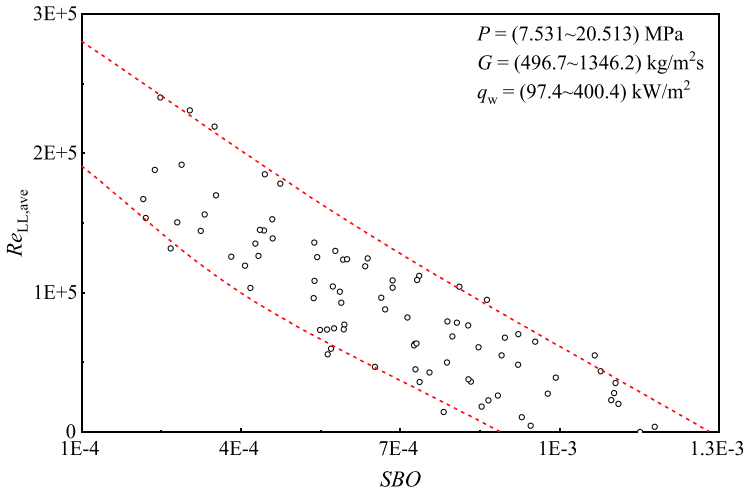

Fig. 11. The relationship between $Re_{LL,ave}$ and *SBO* covering the whole range of experiment data.

0, the h_{exp}/h_{DB} gradually approaches 1 with decreasing x, and in the VL regime with x larger than 1, the h_{exp}/h_{DB} gradually approaches 1 with increasing x. In other words, the heat transfer becomes similar to single-phase convection as the fluid moves away from the TPL regime. The deviation from single-phase in the TPL regime and the approaching of single-phase convection in the LL and VL regimes validate the three-regime-model.

The deviation of sCO_2 heat transfer from the single-phase convection is also observed in the TPL regime for vertical tubes [20,25–27,36–38]. The deviation shows either enhanced or deteriorated heat transfer, resulting in that the h_{exp}/h_{DB} either can be larger than 1, or can be smaller than 1. However, Fig. 12 shows that for horizontal tubes, the deviation in the TPL regime is mostly deteriorated heat transfer, with the h_{exp}/h_{DB} below 1, especially for the top wall. The reason is that the top

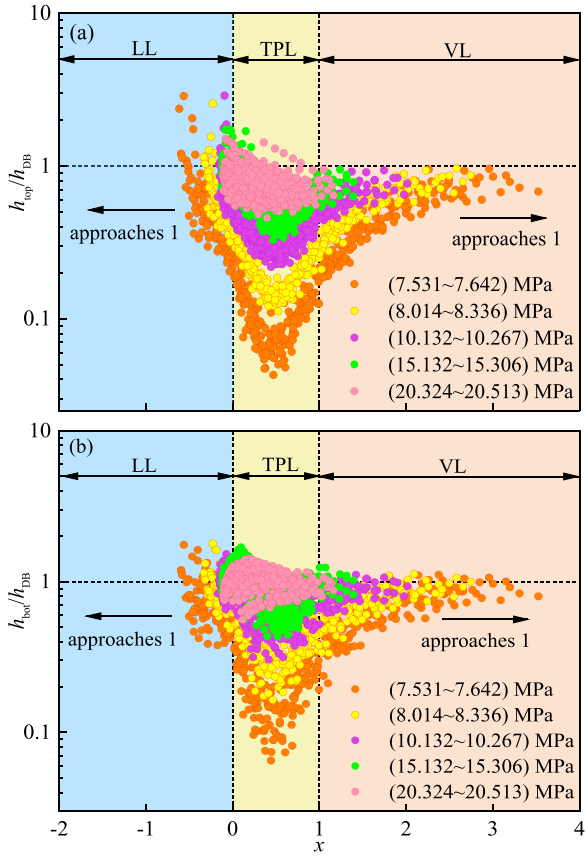

Fig. 12. Deviations of measured heat transfer coefficients from the single-phase convection predictions. (a) h_{top}/h_{DB} versus x; (b) h_{bot}/h_{DB} versus x.

wall tends to have thick VL film due to the stratification effect, hence poor heat transfer takes place there. Moreover, it can be seen from Fig. 12 that with increasing pressure, the deviation from the single-phase DB correlation becomes less prominent with increasing pressure, which is because the latent part of the pseudo-boiling enthalpy becomes smaller with increasing pressures [20–22].

To identify the comprehensive effect of pseudo-boiling and stratification on the heat transfer difference between top and bottom of the tube, Fig. 13 shows h_{bot}/h_{top} and Fr at pressures of 8.065 MPa, 10.153 MPa, and 15.202 MPa, in which Fig. 13(a) shows the schematic drawing of the test tube with the definition of the notations. The horizontal axis is the supercritical pseudo-vapor quality, x, ranging from −0.5 to 0 in the LL regime, 0 to 1 in the TPL regime, and 1 to 2.5 in the VL regime. For all the runs presented in Fig. 13(b-d), the h_{bot}/h_{top} approaches 1 in the LL and VL regimes, indicating the weakened stratification effect due to the single-phase flow in the two regimes. However, in the TPL regime, the h_{bot}/h_{top} obviously deviate from 1. Most of data points for h_{bot}/h_{top} are in the range of 1.5~2.3. Fig. 13(b–d) also shows the variation of Fr against the pseudo-vapor quality. With increasing x, the Fr increases for all cases. In the TPL regime, the $h_{bot}/h_{top}>1$ indicates significant fluid stratification. In the VL regime, the Fr increases along the tube, indicating the dominance of the inertia effect compared to the gravity, so that the heat transfer difference between top and bottom surfaces diminishes, and the ratio of h_{bot}/h_{top} decreases and approaches 1.

5. Conclusions

Major conclusions are summarized as follows:

(1) The outer wall temperatures are found to oscillate along the flow direction, based on which the supercritical fluid is treated separately by a liquid-like core flow and a vapor-like layer on the tube wall. The VL and LL phases form the wavy interface to adapt the oscillation distribution of the wall temperatures.

(2) The oscillation of wall temperatures is explained by the thermal conduction in the solid wall and the stratified-wavy flow. The increase of wall temperatures decreases the local heat flux due to the solid thermal conduction, which decreases the *SBO* there to decrease the vapor-like film thickness, thus the heat transfer can be recovered.

(3) Wall temperatures are different between the top generatrix and the bottom generatrix. A regime map clarifies the positive and negative ΔT runs, using $Fr_{LL,ave}$ and $Fr_{VL,ave}$ as the two coordinates. The maximum wall temperature differences are well correlated versus the liquid-like phase Reynolds number, $Re_{LL,ave}$, or the supercritical boiling number, *SBO*.

(4) The measured heat transfer coefficients, h_{exp}, are compared with the predictions based on the single-phase fluid assumption for supercritical fluids. In the LL and VL regimes, the h_{exp}/h_{DB} approaches 1. But in the TPL regime, the h_{exp}/h_{DB} significantly deviate from 1, suggesting the necessary to introduce the pseudo-boiling theory to treat the supercritical heat transfer.

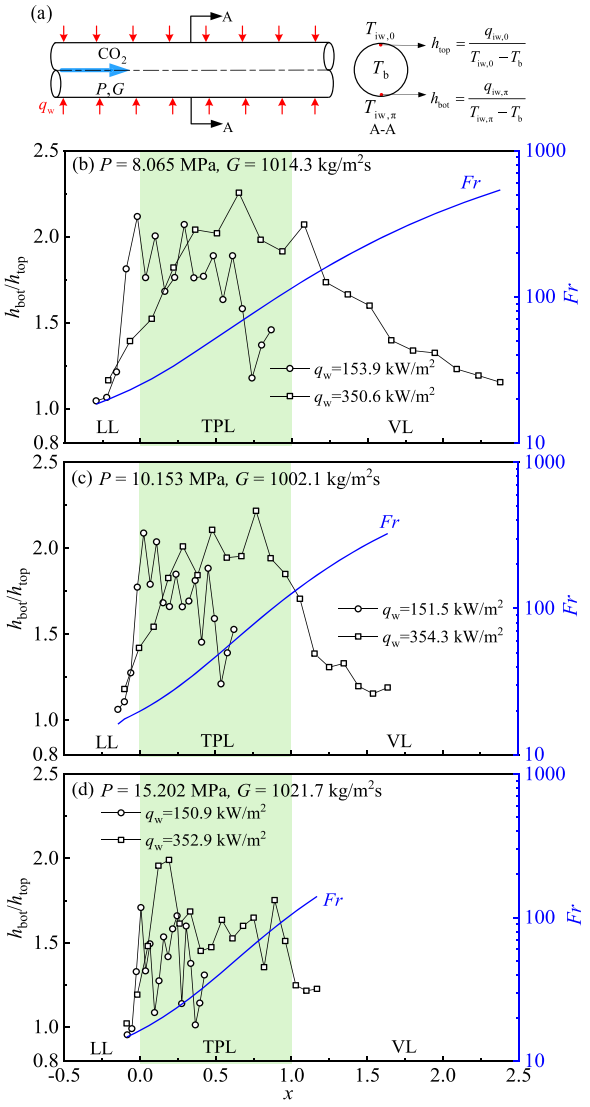

Fig. 13. Effect of x on the difference of heat transfer coefficients between bottom generatrix and top generatrix. (a) definition of parameters; (b) the P=~8 MPa cases; (c) the P=~10 MPa cases; (d) the P=~15 MPa cases.

(5) The h_{bot}/h_{top} approaches 1 in the regimes of LL and VL, but the strong deviation of h_{bot}/h_{top} from 1 indicates both important effects of pseudo-boiling and fluid stratification for horizontal flow in supercritical pressure.

CRediT authorship contribution statement

Liangyuan Cheng: Investigation, Methodology, Software, Validation, Formal analysis, Investigation, Writing – original draft. **Qingyang Wang:** Investigation, Methodology. **Jinliang Xu:** Conceptualization, Supervision, Project administration, Writing – review & editing.

Declaration of Competing Interest

The authors declare that they have no known competing financial interests or personal relationships that could have appeared to influence the work reported in this paper.

Data availability

Data will be made available on request.

Acknowledgments

The authors acknowledge the support from the National Natural Science Foundation of China (No. 52130608 and No. 51821004).

References

[1] J. Xu, E. Sun, M. Li, H. Liu, B. Zhu, Key issues and solution strategies for supercritical carbon dioxide coal fired power plant, Energy 157 (2018) 227–246.
[2] Q. Wang, J. Xu, C. Zhang, B. Hao, L. Cheng, A critical review on heat transfer of supercritical fluids, Heat Transf. Eng. 44 (21) (2023) 1–26.
[3] X.D. Niu, H. Yamaguchi, X.R. Zhang, Y. Iwamoto, N. Hashitani, Experimental study of heat transfer characteristics of supercritical CO_2 fluid in collectors of solar Rankine cycle system, Appl. Therm. Eng. 31 (6) (2011) 1279–1285.
[4] H. Yamaguchi, X.R. Zhang, K. Fujima, M. Enomoto, N. Sawada, Solar energy powered Rankine cycle using supercritical CO_2, Appl. Therm. Eng. 26 (17) (2006) 2345–2354.
[5] G.A. Adebiyi, W.B. Hall, Experimental investigation of heat transfer to supercritical pressure carbon dioxide in a horizontal pipe, Int. J. Heat Mass Transf. 19 (7) (1976) 715–720.
[6] S.R. Pidaparti, J.A. Mcfarland, M.M. Mikhaeil, M.H. Anderson, D. Ranjan, Investigation of buoyancy effects on heat transfer characteristics of supercritical carbon dioxide in heating mode, ASME J of Nucl. Rad Sci (2015).
[7] T. Walisch, M. Müller, W. Dörfler, C. Trepp, The heat transfer to supercritical carbon dioxide in tubes with mixed convection, Process Technol. Proc. 12 (1996) 199–204.
[8] S.M. Liao, T.S. Zhao, An experimental investigation of convection heat transfer to supercritical carbon dioxide in miniature tubes, Int. J. Heat Mass Transf. 45 (25) (2002) 5025–5034.
[9] K. Tanimizu, R. Sadr, Experimental investigation of buoyancy effects on convection heat transfer of supercritical CO_2 flow in a horizontal tube, Heat Mass Transf. 52 (4) (2016) 713–726.
[10] T.H. Kim, J.G. Kwon, M.H. Kim, H.S. Park, Experimental investigation on validity of buoyancy parameters to heat transfer of CO_2 at supercritical pressures in a horizontal tube, Exp. Therm Fluid Sci. 92 (2018) 222–230.
[11] H. Pu, N. Li, M. Dong, Y. Shang, H. Du, C. Hou, J. Zhang, Numerical investigation on turbulent mixed convective heat transfer of CO_2 in a horizontal miniature tube at supercritical pressure, Int. J. Therm. Sci. 184 (2023), 107992.
[12] Z. Zhao, B. Yuan, W. Du, Assessment and modification of buoyancy criteria for supercritical pressure CO_2 convection heat transfer in a horizontal tube, Appl. Therm. Eng. 169 (2020), 114808.
[13] S. Mao, T. Zhou, D. Wei, W. Liu, C. Xue, Numerical investigation on flow and thermal performance of supercritical CO_2 in a horizontal ribbed tube, J. Supercrit. Fluids 187 (2022), 105644.
[14] Z. Zhao, J. Wu, Y. Lin, Q. Xiao, F. Bai, Z. Liu, Y. Liu, M. Tao, C. Dai, Numerical investigation on conjugate heat transfer of supercritical CO_2 in a horizontal double-pipe heat exchanger, in: Proceedings of the 25th International Conference on Nuclear Engineering, 2017.
[15] X. Chu, E. Laurien, Flow stratification of supercritical CO_2 in a heated horizontal pipe, J. Supercrit. Fluids 116 (2016) 172–189.
[16] M. Yang, Numerical study on the heat transfer of carbon dioxide in horizontal straight tubes under supercritical pressure, PLoS One 11 (7) (2016), e0159602.
[17] V.P. Carey, Liquid-Vapor Phase-Change Phenomena, in: An Introduction to the Thermophysics of Vaporization and Condensation Process in Heat Transfer Equipment, Bristol, by Taylor & Francis, 1992.
[18] Y. Ding, S. Kakac, X. Chen, Stratification of boiling two-phase flow in a single horizontal channel, Heat Mass Transf. 30 (3) (1995) 187–195.
[19] Y. Taitel, A.E. Dukler, A model for predicting flow regime transitions in horizontal and near horizontal gas-liquid flow, AIChE J. 22 (1) (1976) 47–55.
[20] Q. Wang, X. Ma, J. Xu, M. Li, Y. Wang, The three-regime-model for pseudo-boiling in supercritical pressure, Int. J. Heat Mass Transf. 181 (2021), 121875.
[21] D. Banuti, Crossing the Widom-line–supercritical pseudo-boiling, J. Supercrit. Fluids 98 (2015) 12–16.
[22] J. Xu, Y. Wang, X. Ma, Phase distribution including a bubblelike region in supercritical fluid, Phys. Rev. E 104 (1) (2021), 014142.
[23] C.H. Son, H.K. Oh, Condensation heat transfer characteristics of CO_2 in a horizontal smooth- and microfin-tube at high saturation temperatures, Appl. Therm. Eng. 36 (2012) 51–62.
[24] L. Cheng, G. Ribatski, J.M. Quibén, J.R. Thome, New prediction methods for CO_2 evaporation inside tubes: part I–a two-phase flow pattern map and a flow pattern based phenomenological model for two-phase flow frictional pressure drops, Int. J. Heat Mass Transf. 51 (1–2) (2008) 111–124.
[25] B. Zhu, J. Xu, C. Yan, J. Xie, The general supercritical heat transfer correlation for vertical up-flow tubes: k number correlation, Int. J. Heat Mass Transf. 148 (2020), 119080.
[26] B. Zhu, J. Xu, X. Wu, J. Xie, M. Li, Supercritical "boiling" number, a new parameter to distinguish two regimes of carbon dioxide heat transfer in tubes, Int. J. Therm. Sci. 136 (2019) 254–266.
[27] H. Zhang, J. Xu, X. Zhu, J. Xie, M. Li, B. Zhu, The K number, a new analogy criterion number to connect pressure drop and heat transfer of sCO_2 in vertical tubes, Appl. Therm. Eng. 182 (2021), 116078.
[28] J. Xu, T. Chen, A nonlinear solution of inverse heat conduction problem for obtaining the inner heat transfer coefficient, Heat Transf. Eng. 19 (2) (1998) 45–53.
[29] B. Zhu, J. Xu, H. Zhang, J. Xie, M. Li, Effect of non-uniform heating on $scCO_2$ heat transfer deterioration, Appl. Therm. Eng. 181 (2020), 115967.
[30] J.P. Holman, Experimental Methods For Engineers, McGraw-Hill, New York, 2012.
[31] J. Xu, H. Zhang, B. Zhu, J. Xie, Critical supercritical-boiling-number to determine the onset of heat transfer deterioration for supercritical fluids, J. Sol. Energy 195 (2020) 27–36.
[32] A. Bar-Cohen, Z. Ruder, P. Griffith, Thermal and hydrodynamic phenomena in a horizontal, uniformly heated steam-generating pipe, J. Heat Transf. 109 (3) (1987) 739–745.
[33] N. Liang, S. Shuangquan, C. Tian, Y.Y. Yan, Two-phase flow instabilities in horizontal straight tube evaporator, Appl. Therm. Eng. 31 (2) (2011) 181–187.
[34] S. Karagoz, S. Karsli, M. Yilmaz, O. Comakli, Density-wave flow oscillations in a water boiling horizontal tube with inserts, J. Enhanc. Heat Transf. 16 (4) (2009).
[35] H. Pan, Q. Bi, W. Tan, P. Yang, F. Feng, Dynamic flow instabilities of hydrocarbon fuel in a horizontal heating tube, Acta Astronaut. 185 (2021) 89–101.
[36] Q. Zhang, H. Li, X. Kong, J. Liu, X. Lei, Special heat transfer characteristics of supercritical CO_2 flowing in a vertically-upward tube with low mass flux, Int. J. Heat Mass Transf. 122 (2018) 469–482.
[37] N. Kline, F. Feuerstein, S. Tavoularis, Onset of heat transfer deterioration in vertical pipe flows of CO_2 at supercritical pressures, Int. J. Heat Mass Transf. 118 (2018) 1056–1068.
[38] Y.Y. Bae, H.Y. Kim, D.J. Kang, Forced and mixed convection heat transfer to supercritical CO_2 vertically flowing in a uniformly-heated circular tube, Exp. Therm. Fluid Sci. 34 (8) (2010) 1295–1308.